THE JOURNAL OF PHYSICAL CHEMISTRY B

ARTICLE

pubs.acs.org/JPCB

Interaction between Lipids and Antimicrobial Oligomers Studied by Solid-State NMR

Weiguo Hu,* Abhigyan Som, and Gregory N. Tew

Department of Polymer Science and Engineering, University of Massachusetts Amherst, Amherst, Massachusetts 01003, United States

Supporting Information

ABSTRACT: Antimicrobial peptides and their synthetic analogues are well known to interact with the cell membrane, which has complex distributions of lipids. The phase behavior of DOPE/DOPG mixed lipids and the interaction between the lipids and several synthetic amphiphilic antimicrobial oligomers (AMOs) were studied by solid-state nuclear magnetic resonance (NMR). A phase diagram of the lipids over a broad window of water content was constructed. There are large areas in the phase diagram where multiple phases coexist, and the fraction of each phase at a given state is dependent on the sample's preparation and thermal history. The comparable stability of the different phases implies that even slight changes in the lipid condition could result in substantial changes to the phase structure, which may be utilized by living organisms to achieve many membrane functions. Nuclear Overhauser spectroscopy (NOESY) and several other NMR experiments indicated that the AMO primarily resides in the head group region of the lipids and that DOPE, the negative intrinsic curvature lipid, does not selectively enrich in the inverted hexagonal phase.

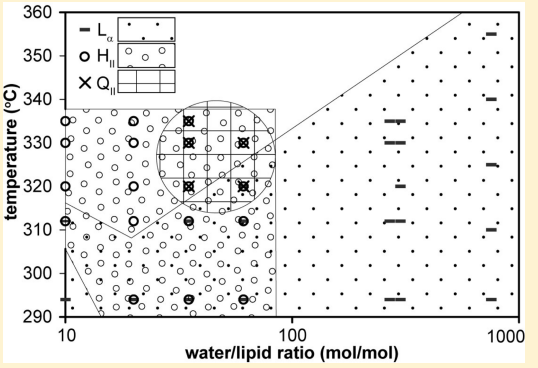

INTRODUCTION

Many plants and animals produce antimicrobial peptides (AMPs) that kill microbial cells mostly by disrupting their cell membranes. They exhibit remarkable selective toxicity toward microbial cell membranes but are relatively safe toward the host cell. AMPs consist of relatively complex structures; hereby, studying their biological activity in simpler structures became an important research objective. This led many research groups to work on novel biomimetic molecules, synthetic mimics of antimicrobial peptides (SMAMPs), which capture the essential chemical and biological properties of AMPs.[1−6] Recently, nonpeptidic triaryl phenylene ethynylene antimicrobial oligomers (AMOs) with tunable structural features similar to those of natural, membrane-spanning AMPs have been synthesized and investigated.[3,7−9]

Various data point to the suggestion that the mechanism of the antibacterial activity is related to the tendency of the bacterial membrane to form an inverted hexagonal phase (H_{II}) in the presence of AMOs.[3,7,8,10] Indeed, the major component of Gram-negative bacteria membranes is phosphatidylethanolamines (PE), a negative intrinsic curvature lipid, which by itself adopts the H_{II} phase at ambient environment. Upon mixing with other lipids such as phosphatidylglycerol (PG), a zero intrinsic curvature lipid, the bacterial membrane assumes a stable lamellar phase at ambient environment, but the H_{II} phase is still apparently within the thermodynamic proximity, being easily stabilized by slight changes such as addition of alkanes, cholesterol, proteins, salt, and so forth.[11−14] This phase versatility of bacteria is believed to be important to biological processes.[10,15]

Many solid-state nuclear magnetic resonance (NMR) methods have been used to probe the various aspects of lipid systems. These include wide-line (static) ^{31}P spectra to probe phase structures, $^{1}H-^{1}H$ NOESY to study the interaction of molecules in the lipids, ^{2}H spectra to study the molecular dynamics of lipid segments, pulsed-field gradient methods to study lateral diffusion, and paramagnetic relaxation enhancement methods to study the insertion depth of foreign molecules,[16−19] to name a few.

Due to the importance of the PE/PG bilayer phase versatility and the fact that AMOs have shown the ability to reorganize them into H_{II} phases, we studied the interaction of two AMOs (termed AMO1 and AMO2; see Supporting Information for structures) with DOPE/DOPG (80/20) liposomes by solid-state NMR. Initially, it was critical to establish a phase diagram of the PE/PG system for several reasons. First, a phase diagram would help to understand the thermodynamics required at the L_α/H_{II} phase transition, which underlies the proposed mechanism of the antibacterial activity of the AMOs. Second, there has not been a systematic phase diagram in the literature for this important lipid composition, especially at the biologically relevant high-water-content window. Finally, NMR experiments require highly concentrated lipid/AMO samples, while the findings must be translated back to biologically relevant concentrations. This necessitates a phase diagram across a broad water content window. The phase diagram was found to be complex,

Received: March 14, 2011
Revised: May 22, 2011
Published: May 25, 2011

with large areas of phase coexists and substantial regions of the cubic phase (Q_{II}). This is consistent with the plasticity of the PE/PG system and its predominance for inverted phases.

It was then possible to understand the interactions of these two AMOs with the PE/PG membrane. Previously, it was reported that AMO1 showed no activity toward either bacterial cells or human red blood cells (RBCs), while AMO2 had a low MIC (minimum inhibitory concentration, 0.8 μg/mL) and high selectivity toward bacterial cells over RBCs (HC_{50}/MIC = 93), even though the two molecules only differ by two CH_2 groups.[20] NMR methods enabled us to study the influence of the two AMOs on the phase structure of the lipids. It also allowed a molecular-level understanding of the interactions between the AMOs and the lipids in the bilayer. Importantly, magic-angle spinning (MAS) sideband analysis demonstrated that the inverted phases were not enriched in PE lipid but remained a mixed lipid phase. This implies that the AMOs do not modify the phase diagram by inducing strong lipid phase separation.

EXPERIMENTAL METHODS

The mixtures of DOPG (1,2-dioleoyl-*sn*-glycero-3-[phospho-*rac*-(1-glycerol)] (sodium salt) and DOPE (1,2-dioleoyl-*sn*-glycero-3-phosphoethanolamine) in the weight ratios of 25:75 and 20:80 were used in this study. This composition range is a first-order mimic for Gram-negative bacterial membranes. All of the lipids were purchased from Avanti Polar Lipids Inc. DOPE and DOPG lipid samples (dissolved in chloroform; total net weight of 50 mg) were mixed in the solution state and then were dried in vacuum overnight to remove chloroform. The resulting lipids formed a thin layer on the surface of a round-bottomed flask. After this stage, lipid samples in three different physical states were prepared, (1) multilamellar vesicle (MLV) dispersions, which were prepared by simply vortexing the mixed lipids and excess D_2O, (2) concentrated unilamellar vesicle (ULV) samples, which were prepared by conducting five freeze−thaw cycles on MLV dispersions and then were progressively dehydrated in vacuum at room temperature for various durations, and (3) gravimetric samples, which were prepared by adding a controlled amount of D_2O to anhydrous lipids. The gravimetric samples were allowed to equilibrate for 2 h at room temperature and were then equilibrated by spinning in a 4 mm rotor for 30 min before the experiments.

In all of the samples, D_2O was used instead of water. Water and D_2O display only minor differences in phase transition temperatures and lattice spacings, which are mostly within the measurement error limits.[11] In the following, the terms D_2O and water will be used interchangeably.

Two AMO molecules were studied in this report, AMO1 and AMO2, which were synthesized and characterized as described previously.[9,20,21] AMOs are not soluble in water; therefore, they were introduced to the lipid/D_2O suspension in their DMSO-d_6 (dimethyl sulfoxide) solution form. The possible effect of DMSO on the lipid phase structure is discussed in the Results section.

All NOESY, ^{13}C, MAS ^{31}P, and part of the wide-line ^{31}P NMR data were acquired on a Bruker DSX300 wide bore NMR spectrometer, with a ^{1}H frequency of 300.12 MHz, a ^{13}C frequency of 75.47 MHz, and a ^{31}P frequency of 121.49 MHz. The samples were placed in 4 mm rotors for NMR experiments. There was no pulsed field gradient capability on the spectrometer; therefore, the basic three-pulse sequence was used for NOESY experiments. Wide-line ^{31}P spectra of lipids with high water content were acquired in a 5 mm broad-band-observed probe on a Bruker Avance 400 MHz high-resolution spectrometer. The ^{31}P chemical shift was calibrated using 85% phosphoric acid. The ^{13}C chemical shift was calibrated by setting the tallest lipid peak at 30 ppm. The temperature was calibrated using pure ethylene glycol. The 8−10 kHz magic angle spinning was used for NOESY; 1.5−4 kHz spinning was used for other experiments. The cross-polarization (CP) contact time was 2 ms.

RESULTS

Phase Behavior of DOPE/DOPG Mixed Lipids. In the liquid-crystalline lamellar phase (L_α), the lipid head groups undergo rapid rotation around the lipid−water interface normal direction. The ^{31}P wide-line NMR spectrum exhibits a typical pattern ("powder pattern") with uniaxial chemical shift tensors.[22] At room temperature, the width of the powder pattern is about 40 ppm, with a downfield shoulder and an upfield tip. As the temperature increases, but before transition to the H_{II} phase occurs, the width of the powder pattern becomes slightly narrower, indicating that the motion of the head groups becomes more isotropic.

The spectrum could be complicated by additional motional freedom of the lipid molecules. In the H_{II} phase, rapid lateral diffusion of the lipid molecules around the cylinder axis generates a powder pattern whose width is half that of the L_α and with an inverted asymmetry.[22] In the inverted cubic phase (Q_{II}),[11,23] the lateral diffusion of the lipid molecules is close to being isotropic, generating a single peak at the isotropic chemical shift position in the ^{31}P spectrum.

For lipid molecules in the L_α phase, if the rate of the vesicle tumbling motion is comparable to the width of the powder pattern, the motion would smear out the tip and shoulder of the pattern. For large multilamellar vesicles (MLVs), the isotropic tumbling is slow enough such that the powder pattern is readily discernible. Upon freeze−thaw or sonication, unilamellar vesicles (ULVs) are formed. These vesicles tumble at a faster rate and thus exhibit a smoothed-out powder pattern or even just a single peak.[22] As water is removed from the lipid suspensions, the vesicles collapse, become more tightly packed, and thus lose much of the tumbling motional freedom. This would result in a sharper tip and shoulder for the ^{31}P powder pattern.

In physiological conditions for bacteria, the bacterial membrane is usually surrounded by abundant water. On the other hand, most phase behavior studies for PE-based lipids have been performed with small water content (0−20 water molecules per lipid). Therefore, it is of interest to examine the phase behavior for PE/PG mixed lipids at higher water content. Figure 1 shows a phase diagram of a DOPE/DOPG (80/20 wt/wt) mixed lipid as a function of hydration level and temperature. The sample with the highest hydration level (lipid/water = 1:755 (mol/mol)) was a MLV dispersion. The sample with the second highest hydration level (lipid/water = 1:300 (mol/mol)) was prepared by vacuum drying the MLV suspension (lipid/water = 1:755 (mol/mol)) at room temperature for ∼20 min. All other samples were prepared by vacuum drying ULV suspensions (lipid/water = 1:755 (mol/mol)) at ambient temperature for various durations, and the amount of water in each sample was determined by a high-precision balance. To examine whether the starting dispersion being MLV or ULV makes any difference in phase behavior, we prepared one condensed MLV and one condensed ULV sample with similar water content (lipid/water = 1:300 and

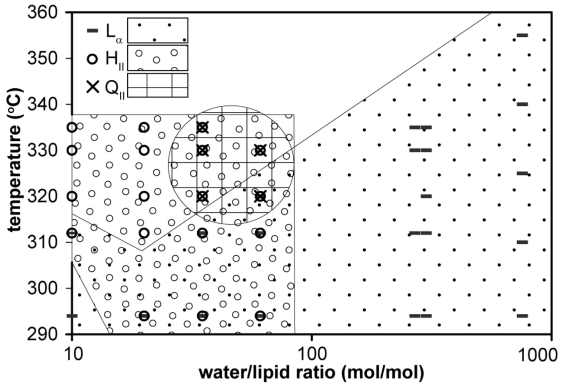

Figure 1. Phase diagram of DOPE/DOPG (80/20) mixed lipids detected by ^{31}P wide-line NMR spectra. The experimental data are represented by large symbols. The continuous areas in which each phase is found are indicated by different shades (dots: L_α; small circles: H_{II}; grids: Q_{II}). The boundaries are approximate and only serve as a guide to the eye.

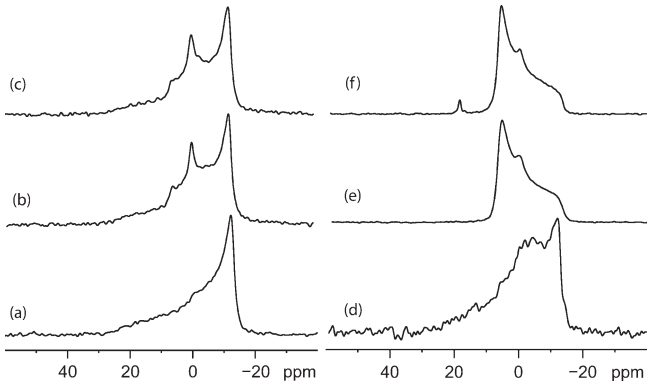

Figure 2. Effect of AMO1, AMO2, and DMSO on the DOPE/DOPG (80/20) mixed lipid phase structure; (a) lipid + DMSO only (same amount of DMSO as that in b and c), (b) lipid + small dosage of AMO1/DMSO solution, (c) lipid + small dosage of AMO2/DMSO solution, (d) lipid + DMSO only (same amount of DMSO as that in e and f), (e) lipid + large dosage of AMO1/DMSO solution, (f) lipid + large dosage of AMO2/DMSO solution. The lipid/AMO ratio is 220:1 (mol/mol) in (b) and (c) and is 20:1 in (e) and (f).

1:270 (mol/mol), respectively) and found their phase behavior to be almost identical.

The identities of phases at each temperature and water content were obtained by ^{31}P wide-line spectra. In the cases where L_α and H_{II} phases coexist, the fraction of each phase was calculated by the following method: A pure L_α line shape was subtracted from the mixed-phase spectrum. The amplitude of the pure L_α line shape was adjusted so that the difference spectrum bore the closest resemblance of a pure H_{II} spectrum. Then, the fraction of the H_{II} phase was calculated as the area ratio of the difference spectrum and the original spectrum. In the cases where Q_{II} and other phases coexist, the signal of the pure Q_{II} phase was simply generated by drawing a baseline at the feet of its peak. The label of a phase is noted on the phase diagram when its population is at least 5% of the total.

Surprisingly complex phase behaviors can be seen in Figure 1. At ambient temperature, the L_α phase is stable at both high water content (200−1000 water molecules per lipid) and low water content (<20 water molecules per lipid). At ambient temperature and intermediate water content (20−100 water molecules per lipid), L_α and H_{II} phases coexist, indicating that both phases are stable at these conditions. At elevated temperatures, the H_{II} phase is more stable at low water content, the Q_{II} phase is more stable at intermediate water content, while the L_α phase at high water content exhibits extraordinary thermal stability. At a water content of 200−300 water molecules per lipid, there was a small amount of Q_{II} phase appearing at higher temperature, but the population did not exceed 5% at any of the temperatures tested.

The phase composition is also apparently dependent on the sample's thermal history. At intermediate water content, the Q_{II} phase is absent in the as-prepared samples at room temperature and appears upon heating. Interestingly, the Q_{II} phase generated this way does not go away when cooled down to room temperature (data not shown in Figure 1). For the lipid/water = 1:60 (mol/mol) sample, we compared the ^{31}P wide-line spectra at 330 K and 3 days after the sample was cooled back to room temperature and found that the fractions of the Q_{II} phase remained about the same. This suggests that the Q_{II} phase is probably as stable as the L_α and H_{II} phases at room temperature, and the relative fractions of the three phases are determined by the sample's thermal history. It is interesting to note that the common perception that the DOPE/DOPG (80/20) mixed lipid is in the lamellar phase at ambient temperature is an overly simplified statement; both H_{II} and Q_{II} phases can stably exist at ambient temperature in broad water content windows.

Sample preparation procedures also apparently affect the observed phase compositions. We prepared two lipid samples at the same lipid/water mole ratio of 1:10, one by adding water to anhydrous lipid ("gravimetric samples") and the other by condensing a MLV dispersion. The former sample is partially in the L_α and partially in the H_{II} phase, while the latter exists entirely in the L_α phase. We also observed that at intermediate water content (20−100 water molecules per lipid), it was very difficult to prepare samples with reproducible phase compositions even with extraordinary care in sample preparation procedures.

Effect of AMOs on Lipid Phase Structures. The DOPE/DOPG mixed lipid with added AMO can also exist in many combinations of phases, including L_α, H_{II}, coexisting L_α + H_{II}, and coexisting H_{II} + Q_{II}. Figure 2 shows the effects of AMO1 and AMO2 on lipid phase structure for MLV dispersions (lipid/water = 1:755 (mol/mol)). Compared to the spectrum in Figure 2a, large changes can be observed in (b) and (c) by adding a very small amount of AMO (lipid/AMO = 220:1 mol/mol). The majority of the new structure is Q_{II}, while the shoulder at ~6 ppm is indicative of a small amount of H_{II} phase. When more AMO is added (Figure 2e and f; lipid/AMO = 20:1), most of the lipid population converts to the H_{II} phase while a minor component transitions into the Q_{II} phase. The H_{II} phase formed upon adding AMO is stable; no appreciable change on the ^{31}P wide-line spectra was found for over 1 week. See the Supporting Information for an investigation of the small, sharp peak at 19 ppm in Figure 2f.

The effect of AMO on the phase structure of condensed lipid samples is less pronounced. As suggested by Figure 1, the condensation process has a strong effect on the lipid phase structure, which would likely mask the effect of AMO.

The AMO molecules in this study are only readily soluble in DMSO; therefore, DMSO has to be introduced into the lipid samples. It is known that DMSO raises the L_β-to-L_α transition temperature and lowers the L_α-to-H_{II} phase transition temperature

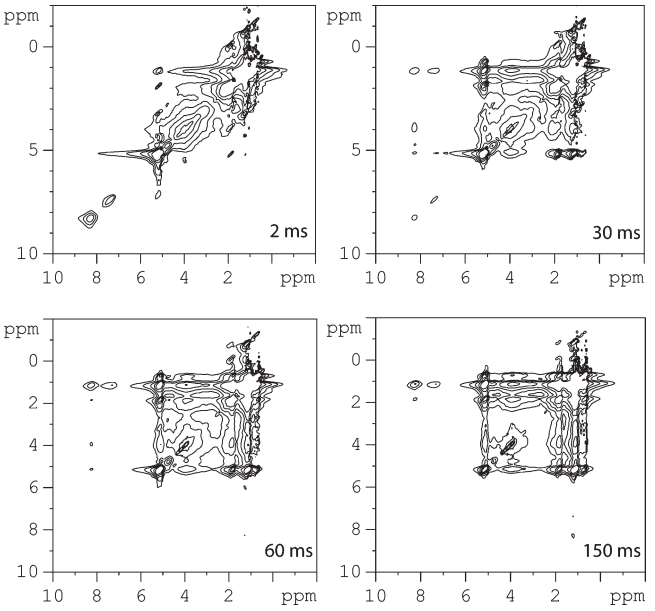

Figure 3. NOESY spectra of DOPE/DOPG mixed lipid (75/25) at 302 K. The MAS speed was 9 kHz. Mixing times are indicated on each spectrum.

of PE lipids.[24] Therefore, for all of the samples with added AMO solution, we also studied control samples with the same amount of DMSO so that the effect of AMO and DMSO could be separated. Comparison of Figure 2a and d suggests that DMSO has some effect on the phase structure at larger dosage; the lamellar powder pattern becomes less well-defined. Nevertheless, the effect of DMSO is obviously much smaller than that of AMO.

The effects of AMO1 and AMO2 on the lipid phase structure for MLV samples appear similar, despite their difference in activity toward Gram-negative bacteria.[7] This suggests that the phase structure changes observed in Figure 2 are due to their structural similarity, likely the dicationic charges, rather than their structural difference (they are different by two methylene groups).

The dicationic charges are also related to the precipitation of lipids when AMO solution is added to the lipid suspensions. The suspension of mixed lipid and water is visibly homogeneous. Upon adding AMO solution, precipitation appears. If only the solvent (DMSO) is added, there is no visible precipitation, suggesting that the precipitation is caused by AMO molecules rather than DMSO solvent. We also observed that the water in the lipid samples with AMO invariably evaporates faster than that in the control in which only DMSO was added to the lipid suspension. The effects of AMO1 and AMO2 on the apparent amount of precipitation are similar, indicating that the precipitation is not related to the antibacterial mechanism but rather to the charge. It has previously been shown that cations can be the fusogenic agents for anionic lipids.[25] The repulsion between the negatively charged lipids maximizes the dispersion of the lipids throughout water, and when AMOs are added, the two positive charges neutralize the lipids and cause the lipid layers to attract more strongly to each other, thus squeezing the water out.

The effect of AMOs on the phase behaviors of PE/PG mixed lipids may be discussed in light of the lipids phase diagram. Figure 1 shows that the L_α phase exhibits extraordinary stability at elevated temperatures, but part of the population readily undergoes phase transition into the H_{II} phase upon removing

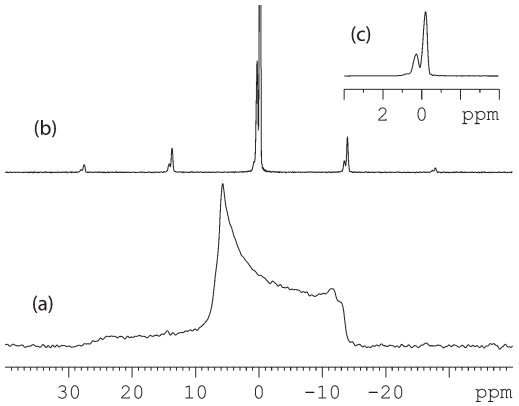

Figure 4. (a) Wide-line and (b) MAS spectra of a mixed lipid sample in the L_α/H_{II} coexisting state; (c) expanded view of the center band in (b).

water. Because AMOs are able to reduce the lipids' affinity to water, their introduction to the lipids moves the physical state leftward on the phase diagram. Figure 2 shows that the lipids partially convert to H_{II} and Q_{II} phases upon adding AMOs, which is qualitatively consistent with the prediction from the phase diagram.

Interaction between AMOs and Lipid Molecules. Figure 3 shows NOESY spectra for a lipid + AMO2 sample (DOPE/DOPG = 75:25 (w/w); lipid/water = 1:25 (mol/mol); lipid/AMO2 = 20:1 (mol/mol)). The sample was in the L_α phase. The t1 ridges were corrected by subtracting an average of a range of signal-free rows from the spectra in the second dimension. Assignment of most peaks can be easily made by comparing with similar lipids.[18] The small peak at 8.3 ppm is from the amine protons of DOPE. The 7.5 ppm peak contains a number of nonequivalent aromatic protons from AMO, but the limited mobility merges the signals into one single broad peak. The peak becomes increasingly sharper at higher temperature, similar to the behavior of the lipid head group signals. Due to the small intensity of the 7.5 ppm peak (its height is about 0.3% of the tallest lipid peak on the ^{1}H spectrum) relative to the t1 ridges, its cross peaks at the lower right half of the spectrum are not reliable. Therefore, our discussions are focused on the cross peaks at the upper left half of the spectrum.

The cross peaks between the 7.5 ppm peak and the major lipid peaks at 1.3 (saturated tail groups), 5.2 (unsaturated tail groups), and 4.0 ppm (head groups) all rise at a fast pace at increasing mixing time. The cross relaxation rates between these groups at short mixing times are similar to that between 1.3 (saturated tail groups) and 4.0 ppm (head groups). This suggests that AMO and the lipids are mixed at the molecular level.

Is PE Enriched in the H_{II} Phase? As the two major components in Gram-negative bacteria membrane, PE and PG have different phase preferences at ambient environment. While the membrane is in the L_α phase most of time, transition into the H_{II} phase is often needed to perform certain biological functions. It would be interesting to investigate whether PE, the negative intrinsic curvature lipid, would selectively enrich in the H_{II} phase upon transition from the L_α phase.

Analysis of MAS sideband patterns of the mixed lipids could provide insight into this question. Due to the different isotropic chemical shifts between PE and PG, their peaks can be resolved in MAS spectra (Figure 4). The distribution of signal intensities on spinning sidebands is determined by chemical shift anisotropy

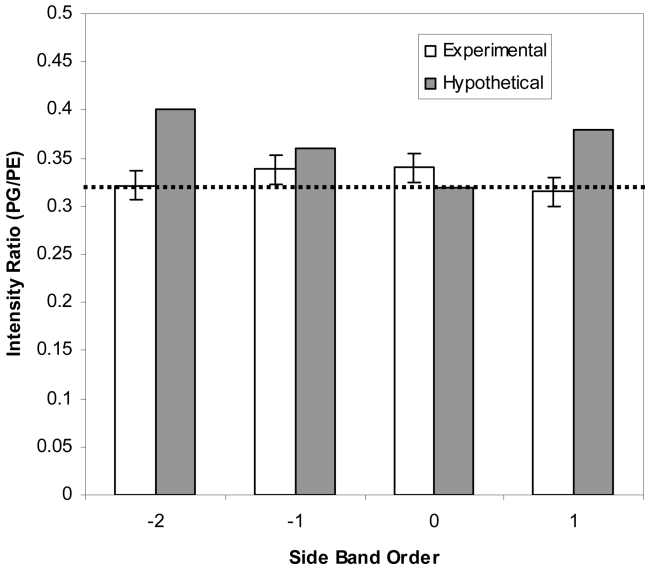

Figure 5. PG/PE peak intensity ratios of the four largest sidebands (including the center band). The experimental results for a PE/PG = 75/25 (wt/wt; or 24/76 (mol/mol)) mixed lipid (experimental series) are very close to the lipid formulation (indicated by the dotted line). If the PE composition (mol/mol) in the H_{II} phase increased to 80% (hypothetical series), the sideband intensity ratios would be substantially different from the experimental results. The error bars represents 5% of the peak intensity ratios.

(CSA). Because L_α and H_{II} phases have different CSAs, their sideband patterns at the same spinning speed are different.

In the L_α phase, the CSA of PE is about 39 ppm, while that of PG is substantially similar.[26] We cannot obtain the CSA of PG in the H_{II} phase because PG does not form the H_{II} phase by itself. However, we can expect that the CSAs of PE and PG in the H_{II} phase are also similar because they are simply half of those in the L_α phase. In a sample consisting of coexisting L_α and H_{II} phases, if PE is enriched in the H_{II} phase, PG must be enriched in the L_α phase. Their sideband patterns would be different from each other, and both would deviate from a prediction based on the lipid composition.

Figure 4a is a wide-line ^{31}P spectrum of a PE/PG (75/25 wt/wt) mixed lipid sample, which is a superposition of L_α and H_{II} powder patterns. The fractions of each phase were determined by the following method: (1) A pure H_{II} spectrum was obtained by subtracting a pure L_α powder pattern (experimental result from another lipid sample) from Figure 4a. It was found to have a signal area that is 54% of the total area. (2) A pure L_α spectrum was obtained by subtracting a pure H_{II} powder pattern (experimental result from another lipid sample) from Figure 4a. It was found to have a signal area that is 42% of the total area. (3) The above two calculations reasonably agree with each other (H_{II} area fraction of 54 versus 58%). The average of the two results in an L_α/H_{II} area ratio of 44:56.

The sideband patterns were then predicted from theoretical calculations based on CSA.[27] We compared the experimental sideband intensity values against the prediction for samples shown in Figure 4, as well as other samples that are in either the pure L_α or H_{II} phase. We found that best fits were obtained when the input CSA for the prediction was 10−15% smaller than what was measured on the wide-line spectra. The difference could be because the lipids powder patterns are motional-averaged patterns from rapidly rotating molecules while the theoretical prediction was based on completely rigid molecules. To minimize the uncertainty due to this disagreement, we drew our conclusions by examining the peak intensity ratio within each sideband order rather than comparing across different sideband orders.

Series 1 of Figure 5 shows the experimental DOPG/DOPE peak intensity ratios for the four largest sidebands, including the center band (order 0). All of the ratios are very close to the lipid mole ratio of 24/76 (corresponding to a weight ratio of 25/75). The data points were plotted with error bars that were 5% of the peak intensity ratios, which was a typical magnitude of error for spinning sideband analysis. Series 2 shows the hypothetical scenario in which the PE/PG ratio in the H_{II} phase slightly deviates from the stoichiometric ratio of 76:24 to 80:20. This would make most of the ratios deviate away from 24/76. This hypothetical scenario is clearly not in agreement with experiment data. This calculation indicates that PE does not substantially enrich in the H_{II} phase in a sample with coexisting $L_\alpha-H_{II}$ phases, which is consistent with the experimental finding of complete miscibility for PE and PG lipids.[28]

DISCUSSION

Phase Behavior of PE/PG Mixed Lipids. There are two interesting features in Figure 1. First is the "re-entrant" phase transition behavior: at ambient temperature, as the water content decreases, the lipids are first in the L_α phase, then in coexisting L_α and H_{II} phases, and then back in the L_α phase. The second feature is the large "gray" area in which multiple phases coexist, or in other words, the lack of sharp phase boundaries. These can be compared with observations for similar lipid systems in the literature. A DOPE−water system was found to exhibit re-entrant phase behavior in a low water content window:[11] at ambient temperature, it is in the H_{II} phase at high (10−20 water per lipid) and low water content (2−6 water per lipid), while in the L_α phase at intermediate water content (6−10 water per lipid). Because mixing of PG with PE lipid raises the L_α-to-H_{II} phase transition temperature, it would be appropriate to compare the ambient-temperature phase behavior in the current study with that of DOPE at a lower temperature. It is reported that mixing 10% DOPG in dielaidoyl phosphatidylethanolamine (DEPE) raised the L_α-to-H_{II} phase transition temperature by ~10 °C.[29] Making a linear extrapolation, the ambient-temperature phase behavior of DOPE/DOPG (80/20 wt/wt) mixed lipids may be comparable to neat DOPE at 0−5 °C. Making this comparison shows that, indeed, they are in agreement; both diagrams point to coexisting L_α/H_{II} phases at >14 waters per lipid and a single L_α phase at 10 waters per lipid.

Similar to Figure 1, there is also a large L_α/H_{II} coexisting area in the DOPE/water phase diagram.[11] For simple molecules such as water and metals, phases usually have sharp boundaries on phase diagrams. For materials comprised of complex molecules, blurry phase boundaries or large phase-coexisting areas are common occurrences. For example, most stereoregular synthetic polymers are partially crystalline and partially amorphous across wide temperature windows despite the large free-energy difference between the crystalline and amorphous phases. This is because the free-energy barrier for phase transition is greater than the free-energy difference between the two phases. The large phase-coexisting area in the lipid phase diagram is likely due to a similar mechanism. Phase transition hysteresis in the DOPE/water phase diagram[11] is consistent with this picture. The free-energy barrier is likely due to the large difference in the supramolecular architecture

for L_α, H_{II}, and Q_{II} phases. The different architectures require extensive molecular reorganization for phase transition to occur. Therefore, it is possible that the free-energy barriers between the phases may be greater than the enthalpies of phase transitions, which are quite small.[11,30]

Because the fractions of the phases of the mixed lipids are dependent on thermal and preparation history, it should be noted that at each data point in Figure 1, there could be more stable phases than what the symbols indicate due to our limited experimental scope. Therefore, Figure 1 should not be regarded as an exhaustive phase diagram. Rather, it simply offers a limited subset of the highly complex phase behavior.

At ambient conditions, for mixed PE/PG lipids with varying composition, the H_{II}/ L_α transition occurs at a PE/PG ratio of ~80/20.[13] This means that at this temperature and composition, the mixed lipids exhibit the smallest preference of being in either phase. Therefore, we can expect that the boundaries on the temperature−water content phase diagram at this composition are rather blurry. This would afford great versatility for biological regulation of phase structures.

H_{II}-forming lipids generally have a "natural" hydration level of ~10 water molecules per lipid at ambient temperature, and a higher hydration level will not further increase the spacing between adjacent lipid layers.[25] Therefore, it seems surprising that the phase diagram in Figure 1 exhibits complex features beyond this natural hydration level. This may be because multiple phases are stable at a given temperature, and which phases the lipids prefer depends on the larger-scale (e.g., 10−1000 nm) architecture of bilayers. Certain phase architectures might be easier to convert to other phases, while other architectures may be more resistant to changes. Although the lipid head groups remain fully hydrated in the entire window of our study, the larger-scale architecture is obviously dependent on water content. As pointed out by Siegel and Epand, during the L_α-to-H_{II} phase transition of dipalmitoleoyl phosphatidylethanolamine (DPPE), the H_{II} phase forms via precursors that have emerged at temperatures tens of degrees below the phase transition temperature.[31] These precursors are connections between apposed bilayers and become more ordered at increasing temperature. This observation suggests that how bilayers are arranged in the dispersion affects the phase transition, which would result in complex phase behavior at high water content, as observed in Figure 1. Several more observations seem to support this view: (1) the fractions of each phase in PE/PG mixed lipids are dependent not only on their physical states but also on their thermal and preparation histories; (2) the L_α phase at the highest water content is stable even at 355 K, while the L_α phase at intermediate water content has mostly converted to H_{II} phase at 310 K.

Location of AMO Molecules in Lipids. Judging from the molecular structure, the AMO molecules in this study are expected to show more affinity with lipid head groups than with tail groups: they have rigid backbones, similar to that for lipid head groups, and they have divalent positive charges, which should be attracted to the negatively charged head groups. Therefore, the AMO molecules are likely to locate near the lipid−water interfaces. Several pieces of evidence support this hypothesis: (1) ^{1}H MAS spectra show that the molecular dynamics of the AMOs, as demonstrated by their aromatic signal (7.5 ppm) width, is similar to that of lipid head groups. (2) ^{31}P MAS peaks of the samples with AMO are broader than the lipid-only controls, while the widths of the tail acyl peaks in the ^{13}C spectra are similar. (3) The precipitation upon adding AMO is likely due to the interaction between the divalent charges of AMO and the negative charges on lipid head groups. These observations are consistent with paramagnetic relaxation enhancement results obtained on similar lipid/AMO systems.[17] They are also consistent with scattering studies performed with AMO2 and lipid monolayers.

Antibacterial Activity Mechanism of AMO Molecules. In this article, we studied two AMO molecules, AMO1, which is nontoxic on Gram-negative bacteria, and AMO2, which is toxic on Gram-negative bacteria but safe on eukaryotic cells.[7] We found that their effects on phase structures of DOPE/DOPG mixed lipid (80/20 wt/wt) are essentially identical within the degree of our method's detectability. This seems contradictory to small-angle X-ray scattering (SAXS) results,[7] which detected diffraction peaks characteristic of the H_{II} phase for DOPE/DOPG (80/20 wt/wt) vesicles with AMO2 but did not find any diffractions for the same lipid with AMO1. We think the seeming disagreement is due to the different nature of SAXS and solid-state NMR methods. SAXS is a sensitive technique, capable of detecting a small fraction of ordered structures out of a large background. ^{31}P wide-line NMR is a bulk detection technique, which means that all of the ^{31}P nuclei in the sample appear in the spectrum. Therefore, small fractions of highly ordered components, which could easily be detected by SAXS, may not appear on a NMR spectrum due to low population.

The H_{II} SAXS diffractions for the lipid sample with AMO2 are quite sharp, indicative of a large and highly ordered crystalline lattice.[7] For H_{II} patterns to appear on a ^{31}P wide-line spectrum, however, no extensive crystalline order is required. We think a possible picture to reconcile SAXS and NMR findings may be that AMO1 and AMO2 are similar in generating phase structural changes for the majority of lipid molecules but AMO2 is uniquely capable of generating a small fraction of highly ordered H_{II} lattice. It remains an open question how this small fraction is responsible for the specific toxicity toward Gram-negative bacteria, but if the more highly ordered lattice is related to long open pore lifetimes, then AMO2 would be more bacteriacidal.

CONCLUSIONS

In DOPE/DOPG (80/20) mixed lipids, multiple phases can coexist across a broad window in the phase diagram, which indicates that several phases have comparable thermal stabilities at or near physiological conditions. Such versatility may be used by certain bacteria to achieve a variety of membrane functions, while novel molecules could be synthesized to take advantage of this property for the defense of many bacteria. A number of NMR experiments show that AMOs are miscible with the lipids at the molecular level and are effective in altering the lipids' phase structure. In mixed DOPE/DOPG lipids that have coexisting L_α and H_{II} phases, both phases have the same lipid composition, indicating no selective enrichment up to our detection limit.

ASSOCIATED CONTENT

Supporting Information. Chemical structures of AMO1 and AMO2 and explanation of the small, sharp peak at 19 ppm in Figure 2f. This material is available free of charge via the Internet at http://pubs.acs.org.

AUTHOR INFORMATION

Corresponding Author

*E-mail: whu@data.pse.umass.edu. Phone: 413 577 1428. Fax: 413 545 0082.

REFERENCES

(1) Liu, D. H.; DeGrado, W. F. *J. Am. Chem. Soc.* **2001**, *123*, 7553.
(2) Sambhy, V.; Peterson, B. R.; Sen, A. *Angew. Chem., Int. Ed.* **2008**, *47*, 1250.
(3) Som, A.; Yang, L. H.; Wong, G. C. L.; Tew, G. N. *J. Am. Chem. Soc.* **2009**, *131*, 15102.
(4) Tew, G. N.; Liu, D. H.; Chen, B.; Doerksen, R. J.; Kaplan, J.; Carroll, P. J.; Klein, M. L.; DeGrado, W. F. *Proc. Natl. Acad. Sci. U.S.A.* **2002**, *99*, 5110.
(5) Tew, G. N.; Scott, R. W.; Klein, M. L.; Degrado, W. F. *Acc. Chem. Res.* **2010**, *43*, 30.
(6) Porter, E. A.; Wang, X. F.; Lee, H. S.; Weisblum, B.; Gellman, S. H. *Nature* **2000**, *404*, 565.
(7) Yang, L. H.; Gordon, V. D.; Mishra, A.; Som, A.; Purdy, K. R.; Davis, M. A.; Tew, G. N.; Wong, G. C. L. *J. Am. Chem. Soc.* **2007**, *129*, 12141.
(8) Yang, L. H.; Gordon, V. D.; Trinkle, D. R.; Schmidt, N. W.; Davis, M. A.; DeVries, C.; Som, A.; Cronan, J. E.; Tew, G. N.; Wong, G. C. L. *Proc. Natl. Acad. Sci. U.S.A.* **2008**, *105*, 20595.
(9) Som, A.; Vemparala, S.; Ivanov, I.; Tew, G. N. *Biopolymers* **2008**, *90*, 83.
(10) Epand, R. M. Membrane Lipid Polymorphism. In *Methods in Membrane Lipids*; Dopico, A. M., Ed.; Humana Press: Totowa, NJ, 2007; p 15.
(11) Gawrisch, K.; Parsegian, V. A.; Hajduk, D. A.; Tate, M. W.; Gruner, S. M.; Fuller, N. L.; Rand, R. P. *Biochemistry* **1992**, *31*, 2856.
(12) Killian, J. A.; van den Berg, C. W.; Tounois, H.; Keur, S.; Slotboom, A. J.; van Scharrenburg, G. J. M.; de Kruijff, B. *Biochim. Biophys. Acta* **1986**, *857*, 13.
(13) Farren, S. B.; Cullis, P. R. *Biochem. Biophys. Res. Commun.* **1980**, *97*, 182.
(14) van der Wel, P. C. A.; Pott, T.; Morein, S.; Greathouse, D. V.; Koeppe, R. E.; Killian, J. A. *Biochemistry* **2000**, *39*, 3124.
(15) Rietveld, A. G.; Killian, J. A.; Dowhan, W.; de Kruijff, B. *J. Biol. Chem.* **1993**, *268*, 12427.
(16) Cullis, P. R.; De Kruijff, B. *Biochim. Biophys. Acta* **1979**, *559*, 399.
(17) Su, Y. C.; DeGrado, W. F.; Hong, M. *J. Am. Chem. Soc.* **2010**, *132*, 9197.
(18) Gaede, H. C.; Gawrisch, K. *Magn. Reson. Chem.* **2004**, *42*, 115.
(19) Huster, D.; Arnold, K.; Gawrisch, K. *J. Phys. Chem. B* **1999**, *103*, 243.
(20) Som, A.; Tew, G. N. *J. Phys. Chem. B* **2008**, *112*, 3495.
(21) Nusslein, K.; Arnt, L.; Rennie, J.; Owens, C.; Tew, G. N. *Microbiol.* **2006**, *152*, 1913.
(22) Smith, I. C. P.; Ekiel, I. H. Phosphorous-31 NMR of Phospholipids in Membranes. In *Phosphorous-31 NMR*; Gorenstein, D. G., Ed.; Academic Press: New York, 1984; p 447.
(23) Foht, P. J.; Tran, Q. M.; Lewis, R. N. A. H.; McElhaney, R. N. *Biochemistry* **1995**, *34*, 13811.
(24) Yu, Z.-W.; Quinn, P. J. *Biochim. Biophys. Acta* **2000**, *1509*, 440.
(25) Arnold, K.; Gawrisch, K. *Methods Enzymol.* **1993**, *220*, 143.
(26) Marassi, F. M.; Macdonald, P. M. *Biochemistry* **1991**, *30*, 10558.
(27) Herzfeld, J.; Berger, A. E. *J. Chem. Phys.* **1980**, *73*, 6021.
(28) Shin, K.-H.; Maeda, H.; Fujiwara, T.; Akutsu, H. *Biochim. Biophys. Acta* **1995**, *1238*, 42.
(29) Tari, A.; Huang, L. *Biochemistry* **1989**, *28*, 7708.
(30) Shalaev, E. Y.; Steponkus, P. L. *Biochim. Biophys. Acta* **1999**, *1419*, 229.
(31) Siegel, D. P.; Epand, R. M. *Biophys. J.* **1997**, *73*, 3089.